frontiers in Physiology

ORIGINAL RESEARCH
published: 05 December 2017
doi: 10.3389/fphys.2017.00997

Modest Static Pressure Suppresses Columnar Epithelial Cell Growth in Association with Cell Shape and Cytoskeletal Modifications

*Man Hagiyama[1], Norikazu Yabuta[2], Daisuke Okuzaki[3], Takao Inoue[1], Yasutoshi Takashima[1], Ryuichiro Kimura[1], Aritoshi Ri[1] and Akihiko Ito[1]**

[1] Department of Pathology, Faculty of Medicine, Kindai University, Osaka-Sayama, Japan, [2] Department of Oncogene Research, Osaka University, Suita, Japan, [3] Genome Information Research Center, Research Institute for Microbial Diseases, Osaka University, Suita, Japan

Intraluminal pressure elevation can cause degenerative disorders, such as ileus and hydronephrosis, and the threshold is fairly low and constant, 20–30 cm H_2O. We previously devised a novel two-chamber culture system subjecting cells cultured on a semipermeable membrane to increased culture medium height (water pressure up to 60 cm H_2O). Here, we sought to determine how a continuous pressure load of ∼30 cm H_2O affects proliferating epithelial cells with special interest in the link with cell morphology. We cultured several different cell lines using the low static pressure-loadable two-chamber system, and examined cell growth, cell cycle, and cell morphology. Madin–Darby canine kidney (MDCK) columnar epithelial cells were growth-suppressed in a manner dependent on static water pressure ranging from 2 to 50 cm H_2O, without cell cycle arrest at any specific phase. Two other types of columnar epithelial cells exhibited similar phenotypes. By contrast, spherical epithelial and mesenchymal cells were not growth-suppressed, even at 50 cm H_2O. Phalloidin staining revealed that 50 cm H_2O pressure load vertically flattened and laterally widened columnar epithelial cells and made actin fiber distribution sparse, without affecting total phalloidin intensity per cell. When the mucosal protectant irsogladine maleate (100 nM) was added to 50-cm-high culture medium, MDCK cells were reduced in volume and their doubling time shortened. Cell proliferation and morphology are known to be regulated by the Hippo signaling pathway. A pressure load of 50 cm H_2O enhanced serine-127 phosphorylation and cytoplasmic retention of YAP, the major constituent of this pathway, suggesting that Hippo pathway was involved in the pressure-induced cell growth suppression. RNA sequencing of MDCK cells showed that a 50 cm H_2O pressure load upregulated *keratin 14*, an intermediate filament, 12-fold. This upregulation was confirmed at the protein level by immunofluorescence, suggesting a role in cytoskeletal reinforcement. These results provide evidence that cell morphology and the cytoskeleton are closely linked to cell growth. Pathological intraluminal pressure elevation may cause mucosal degeneration by acting directly on this linkage and the Hippo pathway.

Keywords: intraluminal pressure, mucosal degeneration, columnar epithelium, slow cell cycle, mechanopathology, two-chamber culture

OPEN ACCESS

Edited by:
Alexander Staruschenko, Medical College of Wisconsin, United States

Reviewed by:
Robert William Hunter, University of Edinburgh, United Kingdom
Masahiro Sokabe, Nagoya University, Japan

****Correspondence:***
Akihiko Ito
aito@med.kindai.ac.jp

Specialty section:
This article was submitted to Renal and Epithelial Physiology, a section of the journal Frontiers in Physiology

Received: *04 September 2017*
Accepted: *20 November 2017*
Published: *05 December 2017*

Citation:
Hagiyama M, Yabuta N, Okuzaki D, Inoue T, Takashima Y, Kimura R, Ri A and Ito A (2017) Modest Static Pressure Suppresses Columnar Epithelial Cell Growth in Association with Cell Shape and Cytoskeletal Modifications. Front. Physiol. 8:997. doi: 10.3389/fphys.2017.00997

INTRODUCTION

Intraluminal pressure exists at various sites in the body, such as the digestive, biliary, and urinary tracts, and intraocular, intracranial, and intraventricular spaces. The normal mean values range approximately from 5 to 20 cm H_2O (Enevoldsen et al., 1976; Schmidt et al., 1978; Coelho et al., 1985; Bratt and Nilsson, 1987; Liu et al., 2003; Kawoos et al., 2015). Increases in intraluminal pressure are thought to cause several diseases and disorders, such as ileus, jaundice, hydronephrosis, hydrocephalus, and glaucoma (Lindahl et al., 1995; Leske et al., 2003; Kumar et al., 2010). These pathological conditions involve degenerative lesions of the mucosa and nervous system, and are known to emerge when intraluminal pressure is persistently elevated over 20–30 cm H_2O (Bratt and Nilsson, 1987; Leske et al., 2003; Kawoos et al., 2015). Thus, the threshold for pressure-induced degeneration is fairly low and constant, regardless of the tissues or organs where the pressure is loaded. This suggests that there is a common mechanism by which such low pressure causes cell and/or tissue degeneration, but the precise molecular basis has not yet been intensively examined.

Recently, we devised a new two-chamber culture system, in which small amounts of water pressure can be loaded on cells without disturbing the standard culture conditions, such as normal pH and partial pressures of oxygen and carbon dioxide (Yoneshige et al., 2017). Using this system, we demonstrated that mouse superior cervical ganglion neurons degenerated when water pressure was over 30 cm H_2O (Yoneshige et al., 2017). Cell adhesion molecule 1, an immunoglobulin superfamily member, appeared to be involved in this neuronal degeneration through increased ectodomain shedding to produce a C-terminal fragment that accumulates in neurites (Yoneshige et al., 2017).

On the other hand, mucosal degeneration associated with intraluminal pressure elevation is thought to involve the retardation of mucosal epithelial renewal, suggesting that pressure directly suppresses epithelial cell proliferation. This speculation is reasonable but its mechanisms have not been carefully examined. The Hippo signaling pathway may be involved because it is crucial for controlling epithelial cell growth by regulating contact inhibition (Gumbiner and Kim, 2014; Yu et al., 2015). This pathway consists of a molecular cascade involving MST2, LATS1, LATS2, YAP, and TAZ (Yu et al., 2015). When the pathway is inactive, YAP is present in the nucleus and transactivates target genes, promoting cell proliferation (Yu et al., 2015). When the pathway is activated, YAP is phosphorylated and retained in the cytoplasm, resulting in suppression of target gene transactivation and cell proliferation (Yu et al., 2015).

Irsogladine maleate (IM) has long been widely used as a mucosal protectant that promotes the healing of gastric ulcers, based on its ability to reinforce epithelial cell adhesion by increasing adhesion-related molecule expression, gap junctional cell–cell communication, and cAMP production (Akagi et al., 2013). Thus, IM may counteract the action of water pressure on epithelial cells.

The aim of the present study is to examine how a continuous pressure load of ∼30 cm H_2O affects proliferating epithelial cells, as we intend to reproduce the *in vivo* process when erosive surfaces of the mucosa are being re-epithelialized by epithelial cell growth under the condition of intraluminal pressure elevation. We had a special interest in cell shape change induced by pressure load, because mucosal epithelia consist generally of columnar-shaped cells. We cultured various types of epithelial and mesenchymal cells using a water pressure-loadable two-chamber system, and examined changes in cell growth profiles and cell morphology. Next, we analyzed protein expression of the Hippo pathway molecules and addressed the Hippo signaling activity, and we comprehensively compared gene expression between pressure-loaded and non-loaded epithelial cells by RNA sequencing. In addition, we examined whether IM rescued the pressure-induced phenomena of epithelial cells. Pressure-induced phenotypes revealed a close link among morphology, cytoskeleton, and proliferation in columnar epithelial cells.

MATERIALS AND METHODS

Cells, Antibodies, and Reagents

Madin–Darby canine kidney (MDCK), NIH3T3, and TIG-1 cells were purchased and cultured as described in our previous reports (Ito et al., 2000, 2008; Hosokawa et al., 2011). Human lung adenocarcinoma NCI-H441 cells (lot no. 58294188) were purchased from the American Type Culture Collection (Manassas, VA, USA) and grown as previously described. Human colon adenocarcinoma Caco-2, and human gastric adenocarcinoma (signet-ring cell carcinoma) KATO-III and NUGC-4 cells were purchased from the Riken BioResource Center, Tsukuba, Japan. All experiments using these cells were performed within 4 months after resuscitation. MDCK, Caco-2, and NCI-H441 cell monolayer cultures on semipermeable membranes were used as representative *in vitro* models of columnar epithelia (Volpe, 2011; Ren et al., 2016). KATO-III and NUGC-4 cells were used as representatives that are of epithelial origin but have a spherical morphology; this morphology well resembles that of signet-ring cell carcinoma cells *in vivo* (Sekiguchi et al., 1978; Nakashio et al., 1997).

Primary antibodies used in this study targeted MST2 (#3952; Cell Signaling, Beverly, MA, USA), LATS1 (C66B5; Cell Signaling), LATS2 (#A300-479A, Bethyl Laboratories, Montgomery, TX, USA), YAP (#4912; Cell Signaling), Phospho-YAP (Ser127; #4911, Cell signaling), TAZ (#HPA007415; Sigma-Aldrich, St. Louis, MO, USA), keratin 14 (LL002; Dako, Glostrup, Denmark), lamin B (M-20; Santa Cruz, Dallas, TX, USA), MCM7 (DCS-141; Medical & Biological Laboratories, Nagoya, Japan), β-actin (Medical & Biological Laboratories), and GAPDH (Medical & Biological Laboratories). Peroxidase-conjugated secondary antibodies used for western blot analysis were purchased from Amersham (Buckinghamshire, England). Phalloidin (rhodamine conjugated) and DAPI were purchased from Molecular Probes (Carlsbad, CA, USA) and Dojindo (Kumamoto, Japan), respectively. IM was kindly provided by Nippon Shinyaku Co., Ltd. (Kyoto, Japan), and was dissolved in DMSO at a concentration of 1 mM (stock solution). Blebbistatin and jasplakinolide were purchased from Wako Pure Chemical Industries (Osaka, Japan) and BioVision, Inc. (San Francisco, CA,

USA), and was dissolved in DMSO at concentrations of 150 and 1.5 mM (stock solution), respectively.

Two-Chamber Culture System for Water Pressure Loading

The water pressure-loadable two-chamber culture device was previously described in detail (Yoneshige et al., 2017). Briefly, the upper chamber composite consisted of a long plastic cylinder with a water-tight connection with a culture insert lined with a semipermeable membrane, and the unit was placed vertically in a 10-cm dish lower chamber. Between the two chambers, a porous (150 μm, 200 cm^2) silicon sheet was inserted to support the semipermeable membrane against the medium (water pressure) applied to the upper chamber cylinder. Using this device, cells were subjected to water pressure levels (cm H_2O) dictated by the height of the medium from the surface to the semipermeable membrane. Partial pressures of oxygen and carbon dioxide and pH were confirmed to be comparable in the upper and lower chambers (Yoneshige et al., 2017).

4×10^4 MDCK or Caco-2 cells, 8×10^4 NCI-H441 cells, and 1×10^5 NIH3T3, TIG-1, KATO-III, or NUGC-4 cells were seeded onto the bottom of a culture insert lined with a semipermeable membrane (transparent PET membrane, pore size 1.0 μm; Corning Life Sciences, Durham, NC, USA) placed in a 6-well plate, and cells were grown in 2-cm-high Eagle's minimum essential medium (EMEM, for MDCK, Caco-2, and TIG-1), RPMI1640 (for NCI-H441, KATO-III, and NUGC-4), or Dulbecco's modified Eagle's medium (DMEM, for NIH3T3) (Wako Pure Chemical Industries) containing 10% fetal bovine serum (FBS). The following day, when the cells grew to ∼40–50% confluency, the insert was set in the pressure-loadable two-chamber system, and the upper and lower chambers were filled with the appropriate medium containing 10% FBS. In some experiments, the IM, blebbistatin or jasplakinolide stock solution or DMSO was added to the upper chamber at 10,000 × (100 nM for IM), 7,500 × (20 μM for blebbistatin) or 75,000 × (20 nM for jasplakinolide) dilution, respectively.

Cell doubling time was calculated as described previously (Nakamoto et al., 2001) with some modifications (see Fluorescent staining and confocal microscopy). Cell cycle analysis was performed using propidium iodide and flow cytometry, as described previously (Ito et al., 2000). Cell viability was examined by trypan blue (0.4 v/w% solution; Wako Pure Chemical Industries) staining. Experiments were done in triplicate, and repeated independently at least three times with essentially similar results.

RNA Sequencing

Total RNA was extracted from MDCK cells cultured in 2- and 50-cm-high media using a miRNeasy Mini Kit (Qiagen, Valencia, CA, USA) according to the manufacturer's protocol. Library preparation was performed using a TruSeq stranded mRNA sample prep kit (Illumina, San Diego, CA, USA) according to the manufacturer's instructions. Sequencing was performed on an Illumina HiSeq 2500 platform in 75-base single-end mode. Illumina Casava 1.8.2 software was used for base-calling. Sequenced reads were mapped to the dog reference genome (CanFam3.1) using TopHat v. 2.0.13 in combination with Bowtie 2 v. 2.2.3 and SAMtools v. 0.1.19. The fragments per kilobase of exon per million mapped fragments (FPKMs) was calculated using Cuffnorm v. 2.2.1. Among the genes calculated with a normalized FPKM value >1.0 in both MDCK cell cultures, 730 genes were more than 2-fold up- or downregulated from the 2-cm H_2O to 50-cm H_2O pressure load. A total of 730 significantly changed genes was queried against functional annotations in the NextBio, Gene Ontology, Broad MSigDB Regulatory Motif, and Broad MSigDB Canonical Pathways databases (http://software.broadinstitute.org/gsea/index.jsp), and more than 100 biological groupings (biogroups) were identified to have a $P < 0.01$ (see Table S2).

Protein Extraction and Western Blot Analysis

Protein extraction from cultured cells and western blot analysis were performed as described previously (Koma et al., 2008). Immunoreactive band intensities were quantified using ImageJ software (National Institutes of Health, Bethesda, MD, USA), as described previously (Mimae et al., 2012).

Fluorescent Staining and Confocal Microscopy

Phalloidin staining and nuclear labeling with DAPI were performed as previously described (Ito et al., 2012; Mimae et al., 2012). Immunofluorescence coupled with phalloidin labeling was performed as previously described (Ito et al., 2012). Briefly, cells were fixed in paraformaldehyde, blocked with 2% bovine serum albumin, and incubated with an antibody against keratin 14 or MCM7, then visualized with Alexa Flour 488-conjugated secondary antibody (anti-mouse IgG; Jackson ImmunoResearch, West Grove, PA, USA). After washing three times with phosphate buffered saline, phalloidin staining was performed for 10 h at 4°C. Nuclei were labeled with DAPI. Fluorescence images were captured using a C2+ confocal scanning system equipped with 488-nm argon and 543-nm helium–neon lasers (Nikon, Tokyo, Japan). The vertical sectional (Z-plane) images were generated by Z-stack confocal microscopy using a 0.4-μm motor step. Captured images were analyzed on the Nikon C2+ computer system using Analysis Controls tools. Length and area were measured with Annotations and Measurements, cell numbers were counted as the number of DAPI-stained nuclei identified using Object Count, and phalloidin intensity (arbitrary unit) was calculated using ROI Statistics. The mean total phalloidin intensity per cell was calculated as follows: in a high-power field view using a 60× objective lens, the total intensities were measured in three XY planes that were in the middle of the Z-axis, and 0.8 μm up and 0.8 μm down, and the mean value was calculated and expressed as phalloidin intensity per XY plane. The total intensity of phalloidin per cell was calculated as follows: the mean phalloidin intensity of 10 randomly selected ZX planes was multiplied by the area of the XY plane, then divided by the cell number. Ten randomly selected high-power field views were examined per experimental group, and the mean and standard

deviation were calculated. In some experiments, Z-projected 3-dimentional images were constructed, and used for analyses of phalloidin intensity (see **Figure 2B**).

To calculate cell doubling time, cells were observed through a 20× objective lens on days 1, 2, and 3 of culture, and total cell numbers per field view were counted as the number of DAPI-stained nuclei identified using Object Count. Ten randomly selected field views were examined per sample, and their mean value was calculated in triplicate cell cultures (30 field views in total) for each day of culture. The mean cell numbers of 3 timepoints were input into Doubling Time Calculator (http://www.doubling-time.com/compute_more.php). The mean and standard deviation of doubling time were calculated by repeating the cell count experiment independently five times.

For assessment of cell proliferation, the number of MCM7-positive nuclei was counted in the randomly selected high-power field views, and its ratio to the total cell number (MCM7 positivity; %) was calculated. The mean ratio and standard deviation were calculated in triplicate experiments.

Statistical Analysis

Differences among experimental groups were analyzed statistically; ANOVA was applied for time-course plots of cell numbers using the software "EZR" (Easy R) (Kanda, 2013), and paired Student's *t*-test for cell doubling time, cell morphological variables, phalloidin and western blot intensities, and immunofluorescence positivity. A $P \leq 0.05$ was considered to indicate statistical significance.

RESULTS

Low Static Pressure Flattens Columnar Epithelial Cells and Suppresses Their Growth

MDCK cells, which are of epithelial origin with a columnar morphology, were cultured on a semipermeable membrane below culture medium that was 2, 15, 30, or 50 cm in height, and the cell numbers were counted after 1, 2, and 3 days. The cell growth curve showed a slow ascent and the doubling time lengthened in a culture medium height-dependent manner (**Figure 1A**). Two other columnar epithelial cell lines, NCI-H441 and Caco-2, and two mesenchymal cell lines, TIG-1 and NIH3T3, were cultured in 2- or 50-cm-high culture medium. NCI-H441 and Caco-2 cells produced results similar to those of MDCK cells (Figures S1A,D), whereas TIG1 and NIH3T3 cells did not exhibit significant differences between the two culture conditions (Figures S2A,C). KATO-III and NUGC-4 cells, which are of epithelial origin but have a spherical morphology, were not growth-suppressed by a static pressure of 50 cm H_2O (Figures S3A,C). Cell cycle profiles of MDCK, NCI-H441, and Caco-2 cells were analyzed by flow cytometry. There were no apparent growth-arrested phases or no appearance of sub-G1 populations detectable in cells in 50-cm-high-medium cultures (**Figure 1B**; Figures S1B,E). Consistent results were obtained by immunofluorescence of MDCK cells against MCM7, a marker for DNA replication; the MCM7-positive cell proportions were comparable between 2- and 50-cm-high-medium cultures (**Figure 1C**). There were practically no MDCK cells positive for trypan blue staining in 50-cm-high-medium cultures. These results suggested that growth suppression in pressure-loaded cells was not due to increased cell death or apoptosis.

Cultured cells were stained with phalloidin. MDCK cells were found to change drastically in shape with the application of a static pressure of 50 cm H_2O. The cell area tripled in the XY plane and the cell height roughly halved in the Z-axis, resulting in 1.5-fold enlargement of the cell volume (cell area × cell height) (**Figure 2A**). Phalloidin staining was markedly weakened in the cytoplasm and on the cell membrane when XY planes around the middle of the Z-axis were observed, but the total intensity per cell was unchanged when the cell volume increase was taken into consideration (**Figures 2A,B**), suggesting that actin fibers became sparsely distributed as the cell volume increased. Similar results were obtained with NCI-H441 and Caco-2 cells (Figures S1C,F). By contrast, in 50-cm-high-medium cultures of KATO-III and NUGC-4 cells, some cells showed a little flattened morphology, but there was no apparent decrease in phalloidin staining intensities (Figures S3B,D). Neither TIG-1 nor NIH3T3 cells exhibited substantial differences in cell shape or phalloidin staining intensity between 2- and 50-cm-high-medium cultures (Figures S2B,D).

Alterations in Protein Expression of Hippo Pathway Molecules by Low Static Pressure

MDCK cells were cultured in 2- or 50-cm-high culture medium for 3 days, and their protein extracts were fractionated into cytosolic and nuclear fractions. Successful fractionation was confirmed by western blot analyses with antibodies against glyceraldehyde 3-phosphate dehydrogenase (GAPDH) and lamin B (**Figure 3**; the original image Figure S4). The duplicate blots were examined for expression of the Hippo pathway molecules, MST2, LATS1, LATS2, YAP, and TAZ. No appreciable differences were detected in the expression levels of the four molecules, i.e., MST2, LATS1, LATS2, or TAZ, between the two culture conditions in either fraction (**Figure 3**). Similar results were obtained with NCI-H441 and Caco-2 cells (**Figure 3**). In contrast, significant differences were detected in the YAP expression. Total YAP levels were decreased in the nuclear fractions of the three cell lines cultured in 50-cm-high medium, and in line with this, serine-127 phosphorylated YAP was increased in their cytoplasmic fractions (**Figure 3**).

Upregulation of Keratin 14 in MDCK Cells by 50 cm H_2O Pressure

RNAs were extracted from MDCK cells cultured in 2- and 50-cm-high culture medium, and gene expression differences were compared by RNA sequencing. The raw data have been deposited in the NCBI Gene Expression Omnibus database (GSE100794). Top 10 up- or down-regulated genes are listed in Table S1. The gene most upregulated in 50-cm-high-medium cultures was *keratin 14*, encoding a type I intermediate filament, with an 11.869-fold change (**Figure 4A**). This upregulation was confirmed at the protein level by western blot analyses

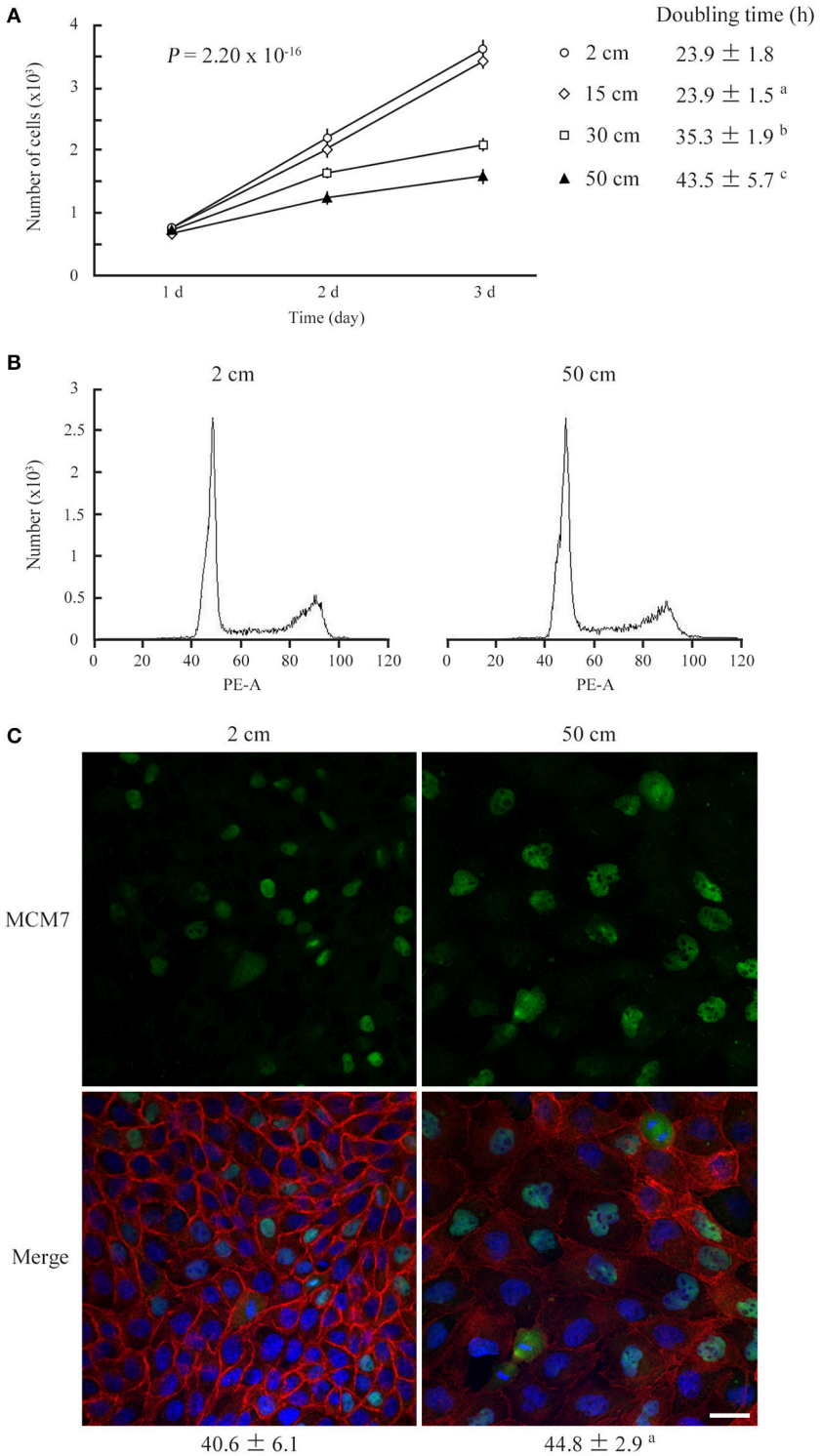

FIGURE 1 | Low static pressure suppresses MDCK cell number increase. **(A)** MDCK cells were cultured on a semipermeable membrane in 2-, 15-, 30-, or 50-cm-high culture medium for 3 days. Cell numbers were counted every day, and the means were plotted with error bars indicating standard deviations ($n = 3$ per group for each experiment). The time-course plots of cell numbers were analyzed by ANOVA; the P-value is shown. Cell doubling time (mean ± standard deviation, hour) was calculated from five independent experiments. $^{a,b,c}P = 0.985$, < 0.001, and < 0.001, respectively, by Student's t-test when compared with 2-cm-high-medium cultures. **(B)** After 3 days of culture in 2- or 50-cm-high medium, MDCK cells were labeled with propidium iodide and analyzed by flow cytometry. Representative results are shown. **(C)** MDCK cells were cultured in 2- or 50-cm-high medium for 3 days, then were triple-stained with MCM7 immunofluorescence (green; upper), phalloidin labeling (red), and DAPI nuclear staining (blue). The three images are merged (lower). MCM7 positivities (mean ± standard deviation, %; $n = 3$ per group) are shown below the photo panels. $^{a}P = 0.208$, by Student's t-test when compared with 2-cm-high-medium cultures. Scale bar = 20 μm.

A

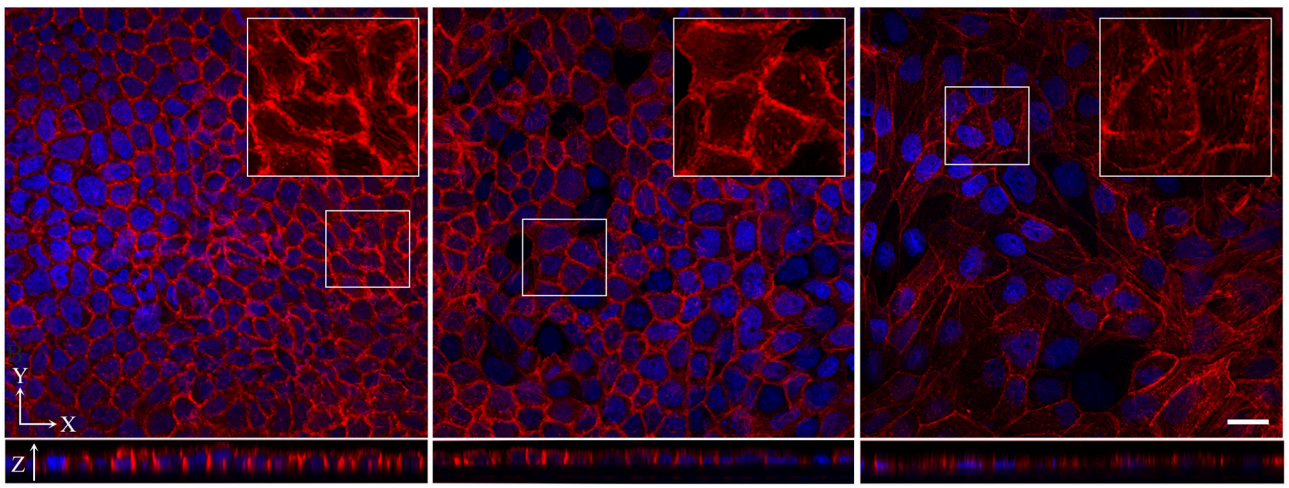

	2 cm	30 cm	50 cm
Cell area (XY; μm^2)	200 ± 40	300 ± 100 [a]	570 ± 230 [a]
Cell hight (Z; μm)	6.53 ± 0.71	4.47 ± 0.72 [a]	3.43 ± 0.49 [a]
Phalloidin intensity (arbitrary unit)			
per XY plane	9450 ± 140	5170 ± 280 [a]	3910 ± 120 [a]
per cell	44.2 ± 1.5	42.2 ± 1.7	45.7 ± 1.0

B

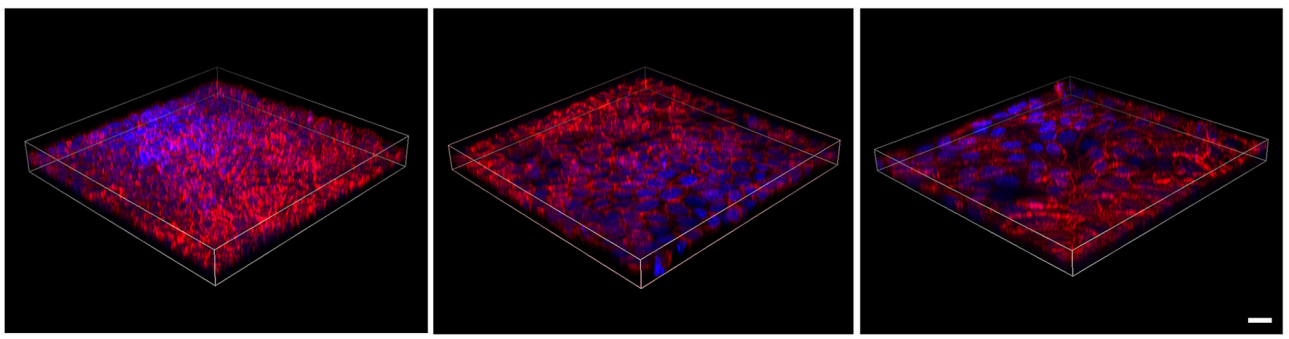

Phalloidin intensity (arbitrary unit)			
per XY plane	17860 ± 350	12710 ± 230 [a]	11650 ± 430 [a]
per cell	336.5 ± 14.4	327.4 ± 7.2	320.7 ± 2.6

FIGURE 2 | Low static pressure flattens epithelial cells in association with diffusion of phalloidin staining. MDCK cells were cultured on a semipermeable membrane in 2-, 30-, or 50-cm-high culture medium for 3 days, and stained with a mixture of phalloidin (red) and DAPI (blue). In **(A)**, cell area and height and phalloidin intensity were measured by laser microscopic examinations. The total intensities of phalloidin per XY plane and per cell were calculated. The former is the mean intensity of three XY planes around the middle of the Z-axis. The latter is calculated as follows: the mean phalloidin intensity of 10 randomly selected ZX planes was multiplied by the area of the XY plane, then divided by the cell number. Boxed areas are enlarged to depict intracellular phalloidin staining, where DAPI fluorescence is not merged. In **(B)**, Z-projected images of MDCK cell monolayers are shown. The total phalloidin intensity contained in each 3-dimentional structure was divided by the cell height and the total cell number present in the monolayer to calculate the phalloidin intensity per XY plane and per cell, respectively. The measured and calculated values (mean ± standard deviation; $n = 3$ per group) are shown below the photo panels. [a]$P \leq 0.001$ by Student's *t*-test when compared with 2-cm-high-medium cultures. Scale bar = 20 μm.

(**Figure 4B**). MDCK cells were double-stained with phalloidin and an anti-keratin 14 antibody. Keratin 14 expression was at trace levels in 2-cm-high-medium cultures, whereas it was clearly detected in the cytoplasm of MDCK cells cultured in 50-cm-high medium, in contrast to a marked decrease in phalloidin staining (**Figure 4C**). Using 730 genes that were more than 2-fold up- or down-regulated from the 2-cm H_2O to 50-cm H_2O pressure load, we performed gene ontology analysis to annotate their biological functions. Gene categories significantly altered ($P < 0.01$) are listed in Table S2. Most significantly up- and down-regulated were the genes associated to transcriptional regulation related to activator protein 1 (AP-1), and those associated to biosynthesis

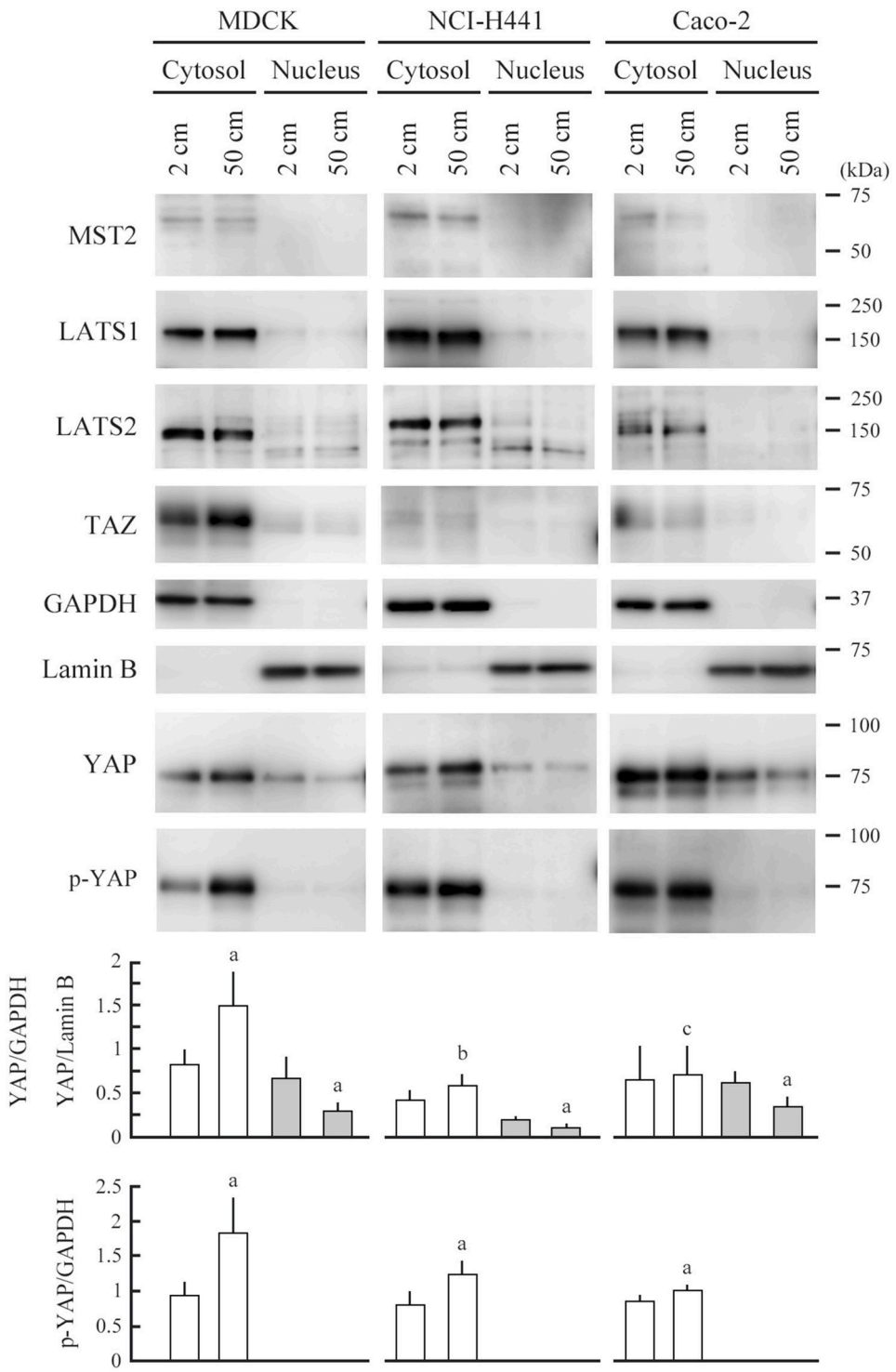

FIGURE 3 | Expression analyses of Hippo pathway molecules. MDCK, NCI-H441, and Caco-2 cells were cultured on a semipermeable membrane in 2- or 50-cm-high medium for 3 days. Cytosolic and nuclear proteins were separately extracted from the cells, and were blotted with the antibodies indicated. Glyceraldehyde 3-phosphate dehydrogenase (GAPDH) and lamin B were used as cytoplasmic and nuclear markers, respectively. Intensities of the immunoreactive bands for YAP, serine-127 phosphorylated YAP (p-YAP), GAPDH, and lamin B were measured densitometrically. The mean ratios of cytosolic YAP and p-YAP to GAPDH (white bar) and nuclear YAP to lamin B (gray bar) and their standard deviations were calculated from the data obtained in three independent experiments. $^{a}P < 0.05$, and $^{b,c}P = 0.213$ and 0.868, respectively, by Student's *t*-test when compared with 2-cm-high-medium cultures.

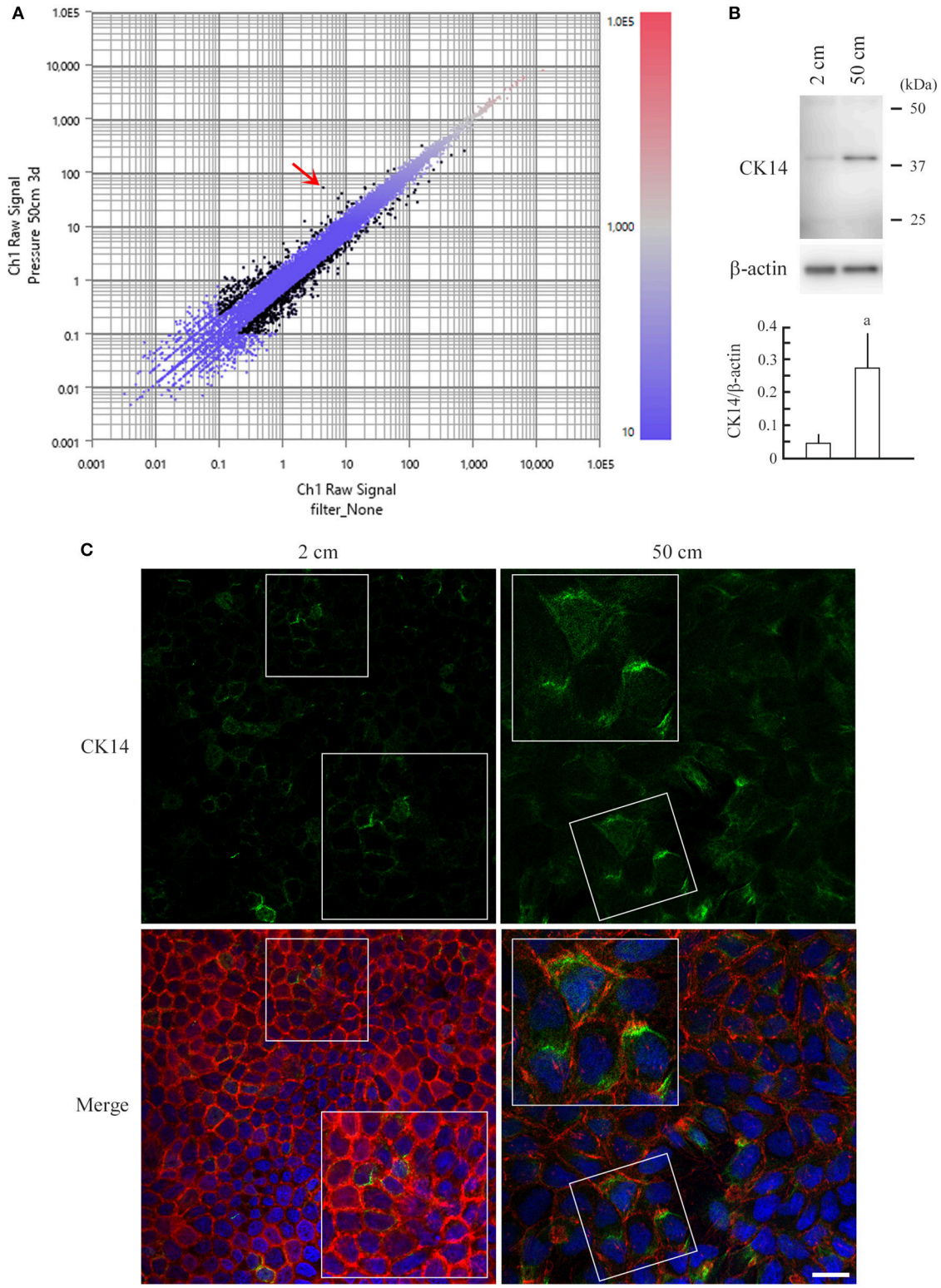

FIGURE 4 | RNA sequencing of MDCK cells and upregulation of keratin 14 in pressure-loaded MDCK cells. **(A)** Total RNA was extracted from MDCK cells that were cultured in 2- or 50-cm-high medium, and was subjected to RNA sequencing-based gene expression comparison analysis. The data are expressed as a scatter plot comparing the $\log_{10}$ fragments per kilobase of exon per million mapped fragments (FPKM) values for 2-cm-high-medium cultures (X-axis) vs. 50-cm-high-medium cultures (Y-axis). The FPKM values are displayed in a red-to-blue gradation, with blue and red indicating the lowest and highest values, respectively. Black dots

(Continued)

FIGURE 4 | indicate genes with >2-fold change. *Keratin 14*, the gene most upregulated in 50-cm-high-medium cultures, with an 11.869-fold change, is indicated with a red arrow. **(B)** MDCK cells were cultured in 2- or 50-cm-high medium, and were subjected to western blot analysis using an anti-keratin 14 antibody (upper panel). The blot was reprobed with an anti-β-actin antibody to indicate the amount of protein loading per lane. Intensities of the immunoreactive bands for keratin 14 and β-actin were measured densitometrically. The mean ratios of keratin 14 to β-actin and standard deviations were calculated from the data obtained in three independent experiments, and were statistically analyzed by Student's *t*-test. $^{a}P = 0.019$ when compared with 2-cm-high-medium cultures. **(C)** MDCK cells were cultured on a semipermeable membrane in 2- or 50-cm-high medium for 3 days, then were triple-stained with keratin 14 immunofluorescence (green; upper), phalloidin labeling (red), and DAPI nuclear staining (blue). The three images are merged (lower). Boxed areas are enlarged to depict keratin 14 upregulation in the cytoplasm of pressure-loaded cells. Scale bar = 20 μm.

and metabolism related to lipids and derivatives, respectively (Table S2).

Pharmacological Assessment of Pressure-Induced Phenomena

MDCK cells were cultured on a semipermeable membrane for 3 days in 2- or 50-cm-high culture medium containing either IM or vehicle (dimethyl sulfoxide, DMSO) alone (final concentrations of IM and DMSO, 100 nM and 10,000× dilution, respectively). Cell doubling times in 2-cm-high-medium cultures were comparable in the IM and vehicle groups, whereas in 50-cm-high-medium cultures, the IM group had a significantly shorter doubling time than the vehicle group (**Figure 5A**). Cell cycle analyses did not indicate any apparent differences between the two groups (**Figure 5B**). MDCK cells were stained with phalloidin. Cell morphology and phalloidin staining intensity were comparable between the IM and vehicle groups in 2-cm-high-medium cultures (**Figure 6**). When cultured in 50-cm-high medium, the IM group had a smaller XY plane cell area, a larger cell height, and a smaller cell volume than the vehicle group (**Figure 6**). IM-treated cells stained more strongly with phalloidin than the vehicle-treated cells, when observed in XY planes around the middle of the Z-axis. The total intensity per cell, however, was comparable in the IM and vehicle groups (**Figure 6**), suggesting that IM did not affect the kinetics of actin polymerization/depolymerization.

We performed similar cell cultures in the presence of either blebbistatin (20 μM), a myosin II inhibitor that relieves F-actin tension, or jasplakinolide (20 nM), an inhibitor of actin filament depolymerization. Both drugs extended the MDCK cell doubling time even in 2-cm-high-medium cultures, consistent with past reports (Senderowicz et al., 1995; Hirata et al., 2017), but blebbistatin, not jasplakinolide, significantly shortened the time in 50-cm-high-medium cultures when compared with DMSO alone (**Figure 5C**; Figure S5).

DISCUSSION

In the present study, we found that relatively small increases in water pressure significantly suppressed the growth of columnar epithelial cells in association with cell height shortening and lateral widening. This cell shape change was associated with decreased intensity of phalloidin staining in the XY plane. By contrast, spherical epithelial-origin cells and mesenchymal cells were not growth-suppressed by the pressure load of 50 cm H_2O, and did not exhibit noticeable changes in cell morphology or phalloidin staining. These results suggest that cell morphological changes and cytoskeletal remodeling are involved in growth suppression induced by modest static pressure, and are consistent with the notion that actin fibers act as a mechano-sensing apparatus (Hayakawa et al., 2011). A pressure of 50 cm H_2O is nearly equal to 0.05 atm = 5 kPa = 5 fN nm^{-2}. Nanometer-sized molecules in live cells fluctuate with forces on the piconewton order because the thermal energy of each molecule at room temperature is on the order of multiplying nanometers by piconewtons ($k_BT = 4.1 \times 10^{-21}$ J = 4.1 pN·nm) (Merkel et al., 1999). This means that under a pressure of 5 fN nm^{-2}, the force loaded on each molecule is fN order, and is too small to perturb the molecular fluctuation. How can cells convert this weak force into biological signals? According to our present study, the primary event caused by the pressure appeared to be cell-shape change, a kind of physical response. This event may trigger particular biological responses, including growth suppression and gene transactivation.

A pressure of 50 cm H_2O made columnar epithelial cells 1.5-fold larger in cell volume, with lateral widening and cell height shortening. This cell volume increase is likely associated with an increase in cell membrane tension. Actin fibers appeared to become sparsely distributed as a result of cell volume increase because their total amount per cell was unchanged. At this time, individual actin fibers may be stretched out, as they have an extensibility as high as 200% (Labouesse et al., 2016). These events may be involved in pressure-induced cell growth retardation. Increased tension of the cell membrane may interfere with the progression of the cell cycle into the S phase because in cells proceeding to cell division, cell volume gradually increases but cell membrane tension remains low (Chang et al., 2014). Sparse distribution and/or stretching of actin fibers may do the same because preexisting actin filaments are used preferentially for the formation of the contractile ring in dividing cells (Cao and Wang, 1990). These notions are supported by the results obtained from adding IM to cultures: when 50 cm H_2O pressure-loaded MDCK cells were treated with IM, their doubling time and cell volume decreased significantly, and phalloidin staining strengthened in the XY planes. Blebbistatin also negated the growth-suppressive effect of 50 cm H_2O pressure load on growing MDCK cells, consistent with the recent studies reporting actin cytoskeletal tension-dependent arrest of epithelial proliferation (Furukawa et al., 2017; Hirata et al., 2017). On the other hand, some past articles clearly demonstrate that stretch-induced membrane/cytoskeletal tension has a promotive effect on epithelial cell proliferation (Aragona et al., 2013; Benham-Pyle et al., 2015). This effect is detected when dense, quiescent monolayers of epithelial cells are stretched, suggesting that it

A

	2 cm		50 cm	
	DMSO	IM	DMSO	IM
MDCK	23.8 ± 0.7	23.7 ± 0.8	44.1 ± 3.8	36.1 ± 1.8 [a]
NCI-H441	38.9 ± 4.2	40.2 ± 2.0	56.7 ± 4.9	48.6 ± 4.9 [b]
Caco-2	35.8 ± 3.8	34.9 ± 4.9	55.5 ± 9.8	45.3 ± 6.6 [b]

B

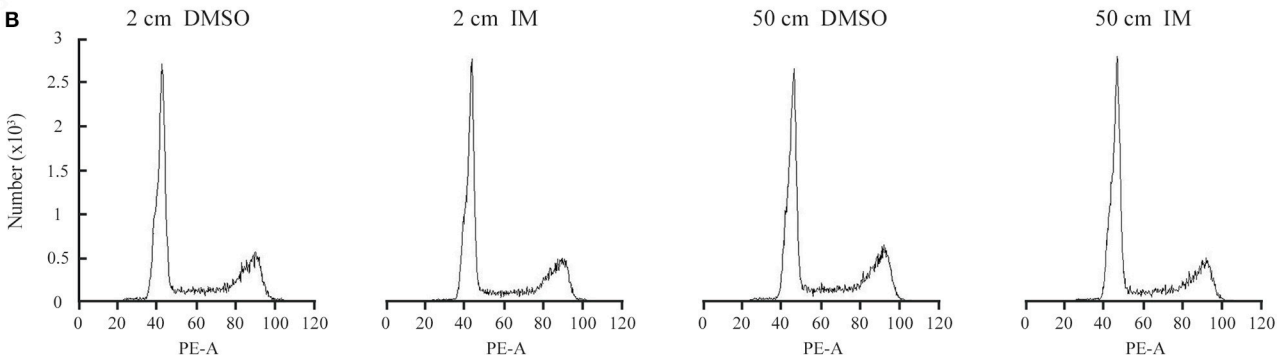

C

	2 cm			50 cm		
	DMSO	Blebbistatin	Jasplakinolide	DMSO	Blebbistatin	Jasplakinolide
MDCK	24.7 ± 1.7	33.8 ± 2.8 [a]	31.6 ± 2.1 [a]	39.6 ± 4.7	30.5 ± 2.2 [a]	37.1 ± 3.3 [b]

FIGURE 5 | Cell growth and cell cycle analyses in the presence of pharmacological agents. **(A)** MDCK, NCI-H441, and Caco-2 cells were cultured in 2- or 50-cm-high medium containing either irsogladine maleate (IM; 100 nM) or DMSO (10,000× dilution), and their doubling times were calculated ($n = 3$ per group for each experiment). The mean and standard deviation (hour) of five independent experiments are shown. [a,b]$P \leq 0.01$ and 0.05, respectively, by Student's *t*-test when compared with the 50 cm DMSO group. **(B)** After 3 days of culture in 2- or 50-cm-high medium, MDCK cells were labeled with propidium iodide and analyzed by flow cytometry. Representative results are shown. **(C)** MDCK cells were cultured in 2- or 50-cm-high medium containing blebbistatin (20 μM), jasplakinolide (20 nM) or DMSO (7,500 × dilution), and their doubling times were calculated ($n = 3$ per group for each experiment). The mean and standard deviation (hour) of five independent experiments are shown. [a,b]$P \leq 0.01$ and $P = 0.371$, respectively, by Student's *t*-test when compared with the 50 cm DMSO group.

stimulates cell cycle reentry. This experimental condition is essentially different from that of the present study, in which cells were loaded with pressure when they should grow actively from sparse cultures to confluent monolayers. Thus, mechanistic force may produce opposite effects on epithelial cells between growth-suppressive or quiescent and proliferative phases.

Notably, YAP appeared to be involved in pressure-induced growth suppression of epithelial cells. YAP is known to bind angiomotin, a component of the intracellular complex of tight junctions, in the back of epithelial lateral membrane (Zhao et al., 2011). The most apparent event induced by static pressure was the lowering of epithelial cell height, i.e., the shortening of the lateral membrane in the Z-axis direction. This structural change in the lateral membrane may activate anigiomotin and/or increase angiomotin–YAP binding, resulting in enhancement of YAP phosphorylation.

RNA sequencing indicated that *keratin 14* was upregulated by modest static pressure in MDCK cells. This upregulation is reasonable because intermediate filaments including keratin 14 act to reinforce cell stiffness and to resist physical strain imposed on the cell (Ma et al., 1999; Nolting et al., 2014). Expression levels of keratin 14 are shown to change dynamically among cell cycle phases, and this change is apparently required for the cell division process to progress (Confalonieri et al., 2017). Constant upregulation of this keratin in MDCK cells can be regarded as one of the causes of cell growth suppression induced by pressure loading. In addition, RNA sequencing suggested that pressure-loaded cells had a general suppression of metabolism and thereby decline in molecular functions. These conditions appear similar to those under starvation. Future studies should clarify the differences between low pressure load, which extends cell doubling time without cell cycle arrest, and starvation, which induces cell cycle arrest at the G1 phase (Cooper, 2003).

Intraluminal pressure elevation often causes the formation of tissue degenerative lesions. Hydronephrosis/obstructive

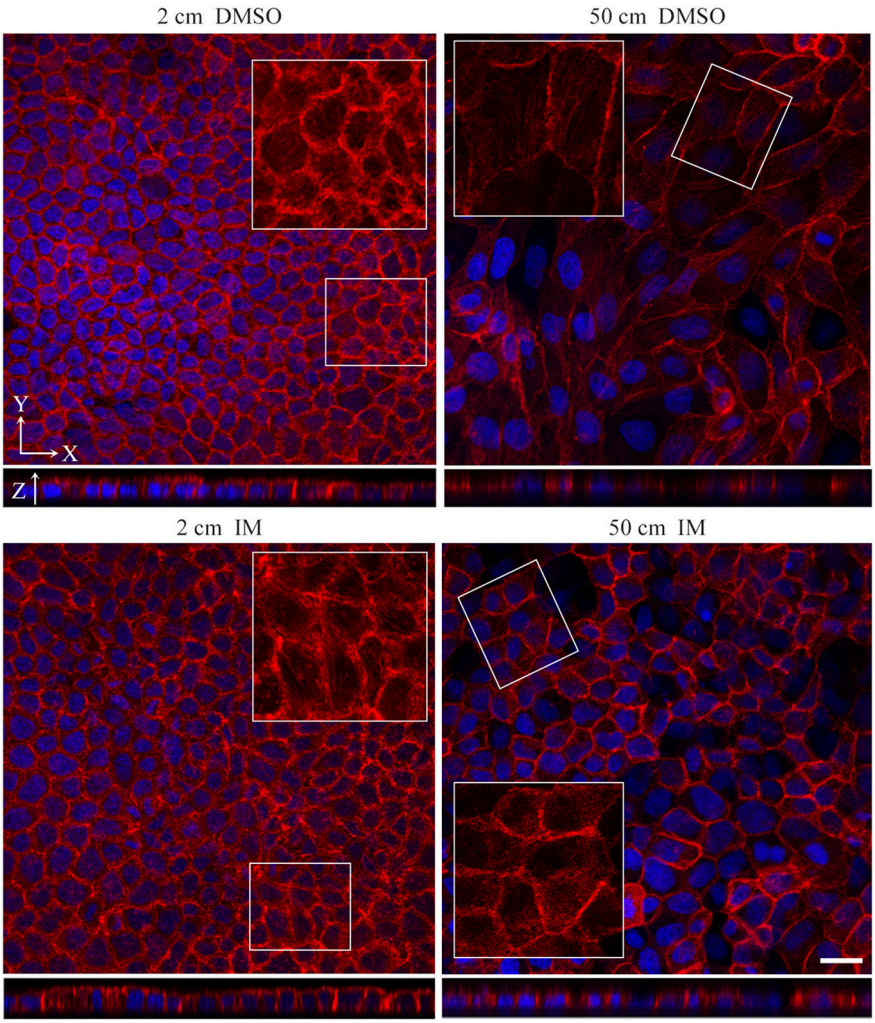

	2 cm DMSO	50 cm DMSO
Cell area (XY; μm²)	200 ± 40	550 ± 220
Cell hight (Z; μm)	6.32 ± 0.78	3.50 ± 0.61
Phalloidin intensity (arbitrary unit)		
per XY plane	9390 ± 140	3880 ± 150
per cell	43.8 ± 0.9	41.6 ± 2.6
	2 cm IM	**50 cm IM**
per XY plane	190 ± 30	310 ± 90 [a]
per cell	6.23 ± 0.78	4.15 ± 0.85 [b]
	9340 ± 200	5190 ± 260 [a]
	42.9 ± 0.9	42.1 ± 0.2

FIGURE 6 | Effects of irsogladine maleate on cell morphology and phalloidin staining. MDCK cells were cultured on a semipermeable membrane for 3 days in 2- or 50-cm-high medium containing either irsogladine maleate (IM; 100 nM) or DMSO (10,000 × dilution), and stained with a mixture of phalloidin (red) and DAPI (blue). Cell area and height and phalloidin intensity were measured by laser microscopic examinations. The total intensities of phalloidin per XY plane and cell were calculated. The former is the mean intensity of three XY planes around the middle of the Z-axis. The latter is caluculated as follows: the mean phalloidin intensity of 10 randomly selected ZX planes was multiplied by the area of the XY plane, then divided by the cell number. Boxed areas are enlarged to depict intracellular phalloidin staining, where DAPI fluorescence is not merged. Shown below the photo panels are the measured and calculated values (mean ± standard deviation; $n = 3$ per group). [a,b]$P \leq 0.01$ and 0.05, respectively, by Student's *t*-test when compared with the 50 cm DMSO group. Scale bar = 20 μm.

nephropathy leads to renal tubular injury through urinary intraluminal pressure increase (Bratt and Nilsson, 1987; Kipari et al., 2006). Obstruction of pancreatic and biliary ducts results in ductal dilatation through intraductal pressure elevation (Turowski et al., 2011). Mechanical ventilation often leads to alveolar damage through excess airway pressure (Cabrera-Benítez et al., 2012). Delayed tissue regeneration and re-epithelialization are assumed to underlie the development of these lesions (Kipari et al., 2006; Turowski et al., 2011; Cabrera-Benítez et al., 2012). Intraluminal pressure elevation can be a direct cause of delayed tissue regeneration/re-epithelialization through the suppression of epithelial cell proliferation. The present study identified IM as a potent drug that can protect against degenerative lesion formation.

In conclusion, the growth of columnar epithelial cells appeared to be suppressed by a static pressure burden as low as a few tens of cm H_2O. The precise mechanisms by which cells can sense such modest pressure remain unknown; however, this study highlights an important role for mutual links among the cytoskeleton, cell morphology and Hippo pathway in the proliferative responses of epithelial cells to modest pressure. These links may underlie a general mechanism of the development and progression of columnar epithelial degeneration and the delay in re-epithelialization of erosive mucosa under pathological conditions of intraluminal pressure elevation.

DATA AVAILABILITY

The raw data of RNA sequencing are deposited in the NCBI Gene Expression Omnibus database (accession number, GSE100794). The URL is as follows https://www.ncbi.nlm.nih.gov/geo/query/acc.cgi?acc=GSE100794.

AUTHOR CONTRIBUTIONS

MH: carried out the cell culture, cell staining, western blotting, and laser microscopic examinations, and performed the statistical analyses; TI, YT, RK, and AR: participated in the western blot analysis and microscopic examinations; NY: supervised the western blot analysis and data interpretation; DO: carried out RNA sequencing and deposited the data into the public database; AI: conceived and designed the study, and drafted the manuscript. All authors read and approved the final manuscript.

FUNDING

This study was supported by Japan Society for the Promotion of Science KAKENHI grants (15K19079, 17K08680 to MH, and 15K15113 to AI); the Ministry of Education, Culture, Sports, Science and Technology-Supported Program for the Strategic Research Foundation at Private Universities 2015-17 (to AI); a twenty-first Century Joint Research Enhancement Grant of Kindai University (to AI); and the Grant for Joint Research Projects of the Research Institute for Microbial Diseases, the University of Osaka (to AI).

SUPPLEMENTARY MATERIAL

The Supplementary Material for this article can be found online at: https://www.frontiersin.org/articles/10.3389/fphys.2017.00997/full#supplementary-material

REFERENCES

Akagi, M., Amagase, K., Murakami, T., and Takeuchi, K. (2013). Irsogladine: overview of the mechanisms of mucosal protective and healing-promoting actions in the gastrointestinal tract. *Curr. Pharm.* 19, 106–114. doi: 10.2174/1381612811306010106

Aragona, M., Panciera, T., Manfrin, A., Giulitti, S., Michielin, F., Elvassore, N., et al. (2013). A mechanical checkpoint controls multicellular growth through YAP/TAZ regulation by actin-processing factors. *Cell* 154, 1047–1059. doi: 10.1016/j.cell.2013.07.042

Benham-Pyle, B. W., Pruitt, B. L., and Nelson, W. J. (2015). Mechanical strain induces E-cadherin-dependent Yap1 and β-catenin activation to drive cell cycle entry. *Science* 348, 1024–1027. doi: 10.1126/science.aaa4559

Bratt, C. G., and Nilsson, S. (1987). Intrapelvic pressure and caliceal dilatation in the evaluation of intermittent hydronephrosis. *J. Urol.* 137, 845–848. doi: 10.1016/S0022-5347(17)44270-4

Cabrera-Benítez, N. E., Parotto, M., Post, M., Han, B., Spieth, P. M., Cheng, W. E., et al. (2012). Mechanical stress induces lung fibrosis by epithelial-mesenchymal transition. *Crit. Care Med.* 40, 510–517. doi: 10.1097/CCM.0b013e31822f09d7

Cao, L. G., and Wang, Y. L. (1990). Mechanism of the formation of contractile ring in dividing cultured animal cells. I. recruitment of preexisting actin filaments into the cleavage furrow. *J. Cell Biol.* 110, 1089–1095. doi: 10.1083/jcb.110.4.1089

Chang, T. H., Huang, H. D., Ong, W. K., Fu, Y. J., Lee, O. K., Chien, S., et al. (2014). The effects of actin cytoskeleton perturbation on keratin intermediate filament formation in mesenchymal stem/stromal cells. *Biomaterials* 35, 3934–3944. doi: 10.1016/j.biomaterials.2014.01.028

Coelho, J. C., Moody, F. G., and Senninger, N. (1985). A new method for correlating pancreatic and biliary duct pressures and sphincter of Oddi electromyography. *Surgery* 97, 342–349.

Confalonieri, M., Buratti, E., Grassi, G., Bussani, R., Chilosi, M., Farra, R., et al. (2017). Keratin14 mRNA expression in human pneumocytes during quiescence, repair and disease. *PLoS ONE* 12:e0172130. doi: 10.1371/journal.pone.0172130

Cooper, S. (2003). Reappraisal of serum starvation, the restriction point, G0, and G1 phase arrest points. *FASEB J.* 17, 333–340. doi: 10.1096/fj.02-0352rev

Enevoldsen, E. M., Cold, G., Jensen, F. T., and Malmros, R. (1976). Dynamic changes in regional CBF, intraventricular pressure, CSF pH and lactate levels during the acute phase of head injury. *J. Neurosurg.* 44, 191–214. doi: 10.3171/jns.1976.44.2.0191

Furukawa, K. T., Yamashita, K., Sakurai, N., and Ohno, S. (2017). The epithelial circumferential actin belt regulates YAP/TAZ through nucleocytoplasmic shuttling of merlin. *Cell Rep.* 20, 1435–1447. doi: 10.1016/j.celrep.2017.07.032

Gumbiner, B. M., and Kim, N. G. (2014). The Hippo-YAP signaling pathway and contact inhibition of growth. *J. Cell Sci.* 127, 709–707. doi: 10.1242/jcs.140103

Hayakawa, K., Tatsumi, H., and Sokabe, M. (2011). Actin filaments function as a tension sensor by tension-dependent binding of cofilin to the filament. *J. Cell Biol.* 195, 721–727. doi: 10.1083/jcb.201102039

Hirata, H., Samsonov, M., and Sokabe, M. (2017). Actomyosin contractility provokes contact inhibition in E-cadherin-ligated keratinocytes. *Sci. Rep.* 7:46326. doi: 10.1038/srep46326

Hosokawa, Y., Hagiyama, M., Iino, T., Murakami, Y., and Ito, A. (2011). Noncontact estimation of intercellular breaking force using a femtosecond laser impulse quantified by atomic force microscopy. *Proc. Natl. Acad. Sci. U.S.A.* 108, 1777–1782. doi: 10.1073/pnas.1006847108

Ito, A., Hagiyama, M., Mimura, T., Matsumoto, M., Wakayama, T., Iseki, S., et al. (2008). Expression of cell adhesion molecule 1 in malignant pleural mesothelioma as a cause of efficient adhesion and growth on mesothelium. *Lab. Invest.* 88, 504–514. doi: 10.1038/labinvest.2008.15

Ito, A., Kataoka, T. R., Watanabe, M., Nishiyama, K., Mazaki, Y., Sabe, H., et al. (2000). A truncated isoform of the PP2A B56 subunit promotes cell motility through paxillin phosphorylation. *EMBO J.* 19, 562–571. doi: 10.1093/emboj/19.4.562

Ito, A., Mimae, T., Yamamoto, Y. S., Hagiyama, M., Nakanishi, J., Ito, M., et al. (2012). Novel application for pseudopodia proteomics using excimer laser ablation and two-dimensional difference gel electrophoresis. *Lab. Invest.* 92, 1374–1385. doi: 10.1038/labinvest.2012.98

Kanda, Y. (2013). Investigation of the freely available easy-to-use software 'EZR' for medical statistics. *Bone Marrow Transplant.* 48, 452–458. doi: 10.1038/bmt.2012.244

Kawoos, U., McCarron, R. M., Auker, C. R., and Chavko, M. (2015). Advances in intracranial pressure monitoring and its significance in managing traumatic brain injury. *Int. J. Mol. Sci.* 16, 28979–28997. doi: 10.3390/ijms161226146

Kipari, T., Cailhier, J. F., Ferenbach, D., Watson, S., Houlberg, K., Walbaum, D., et al. (2006). Nitric oxide is an important mediator of renal tubular epithelial cell death *in vitro* and in murine experimental hydronephrosis. *Am. J. Pathol.* 169, 388–399. doi: 10.2353/ajpath.2006.050964

Koma, Y., Furuno, T., Hagiyama, M., Hamaguchi, K., Nakanishi, M., Masuda, M., et al. (2008). Cell adhesion molecule 1 is a novel pancreatic-islet cell adhesion molecule that mediates nerve-islet cell interactions. *Gastroenterology* 134, 1544–1554. doi: 10.1053/j.gastro.2008.01.081

Kumar, V., Abbas, A. K., Fausto, N., and Aster, J. C. (2010). *Robbins and Cotran Pathologic Basis of Disease, 8th Edn*. Philadelphia, PA: Saunders.

Labouesse, C., Gabella, C., Meister, J. J., Vianay, B., and Verkhovsky, A. B. (2016). Microsurgery-aided *in-situ* force probing reveals extensibility and viscoelastic properties of individual stress fibers. *Sci. Rep.* 6:23722. doi: 10.1038/srep23722

Leske, M. C., Heijl, A., Hussein, M., Bengtsson, B., Hyman, L., and Komaroff, E. (2003). Factors for glaucoma progression and the effect of treatment: the early manifest glaucoma trial. *Arch. Ophthalmol.* 121, 48–56. doi: 10.1001/archopht.121.1.48

Lindahl, O. A., Bäcklund, T., and Sjödin, J. G. (1995). Monitoring of renal pelvic pressure in patients with hydronephrosis. *Physiol. Meas.* 16, 169–179. doi: 10.1088/0967-3334/16/3/004

Liu, J. H., Bouligny, R. P., Kripke, D. F., and Weinreb, R. N. (2003). Nocturnal elevation of intraocular pressure is detectable in the sitting position. *Invest. Ophthalmol. Vis. Sci.* 44, 4439–4442. doi: 10.1167/iovs.03-0349

Ma, L., Xu, J., Coulombe, P. A., and Wirtz, D. (1999). Keratin filament suspensions show unique micromechanical properties. *J. Biol. Chem.* 274, 19145–19151. doi: 10.1074/jbc.274.27.19145

Merkel, R., Nassoy, P., Leung, A., Ritchie, K., and Evans, E. (1999). Energy landscapes of receptor-ligand bonds explored with dynamic force spectroscopy. *Nature* 397, 50–53. doi: 10.1038/16219

Mimae, T., Okada, M., Hagiyama, M., Miyata, Y., Tsutani, Y., Inoue, T., et al. (2012). Upregulation of notch2 and six1 is associated with progression of early-stage lung adenocarcinoma and a more aggressive phenotype at advanced stages. *Clin. Cancer Res.* 18, 945–955. doi: 10.1158/1078-0432.CCR-11-1946

Nakamoto, K., Ito, A., Watabe, K., Koma, Y., Asada, H., Yoshikawa, K., et al. (2001). Increased expression of a nucleolar Nop5/Sik family member in metastatic melanoma cells: evidence for its role in nucleolar sizing and function. *Am. J. Pathol.* 159, 1363–1374. doi: 10.1016/S0002-9440(10)62523-0

Nakashio, T., Narita, T., Sato, M., Akiyama, S., Kasai, Y., Fujiwara, M., et al. (1997). The association of metastasis with the expression of adhesion molecules in cell lines derived from human gastric cancer. *Anticancer Res.* 17, 293–299.

Nolting, J. F., Möbius, W., and Köster, S. (2014). Mechanics of individual keratin bundles in living cells. *Biophys. J.* 107, 2693–2699. doi: 10.1016/j.bpj.2014.10.039

Ren, H., Birch, N. P., and Suresh, V. (2016). An Optimised human cell culture model for alveolar epithelial transport. *PLoS ONE* 11:e0165225. doi: 10.1371/journal.pone.0165225

Schmidt, E., Bruch, H. P., and Laven, R. (1978). Colon dynamics in ileus. *Chirurg.* 49, 104–110.

Sekiguchi, M., Sakakibara, K., and Fujii, G. (1978). Establishment of cultured cell lines derived from a human gastric carcinoma. *Jpn. J. Exp. Med.* 48, 61–68.

Senderowicz, A. M., Kaur, G., Sainz, E., Laing, C., Inman, W. D., Rodríguez, J., et al. (1995). Jasplakinolide's inhibition of the growth of prostate carcinoma cells *in vitro* with disruption of the actin cytoskeleton. *J. Natl. Cancer Inst.* 87, 46–51. doi: 10.1093/jnci/87.1.46

Turowski, C., Knisely, A. S., and Davenport, M. (2011). Role of pressure and pancreatic reflux in the aetiology of choledochal malformation. *Br. J. Surg.* 98, 1319–1326. doi: 10.1002/bjs.7588

Volpe, D. A. (2011). Drug-permeability and transporter assays in Caco-2 and MDCK cell lines. *Future Med. Chem.* 3, 2063–2077. doi: 10.4155/fmc.11.149

Yoneshige, A., Hagiyama, M., Inoue, T., Tanaka, T., Ri, A., and Ito, A. (2017). Modest static pressure can cause enteric nerve degeneration through ectodomain shedding of cell adhesion molecule 1. *Mol. Neurobiol.* 54, 6378–6390. doi: 10.1007/s12035-016-0166-y

Yu, F. X., Zhao, B., and Guan, K. L. (2015). Hippo Pathway in organ size control, tissue homeostasis, and cancer. *Cell* 163, 811–828. doi: 10.1016/j.cell.2015.10.044

Zhao, B., Li, L., Lu, Q., Wang, L. H., Liu, C. Y., Lei, Q., et al. (2011). Angiomotin is a novel Hippo pathway component that inhibits YAP oncoprotein. *Genes Dev.* 25, 51–63. doi: 10.1101/gad.2000111

Conflict of Interest Statement: The authors declare that the research was conducted in the absence of any commercial or financial relationships that could be construed as a potential conflict of interest.

Copyright © 2017 Hagiyama, Yabuta, Okuzaki, Inoue, Takashima, Kimura, Ri and Ito. This is an open-access article distributed under the terms of the Creative Commons Attribution License (CC BY). The use, distribution or reproduction in other forums is permitted, provided the original author(s) or licensor are credited and that the original publication in this journal is cited, in accordance with accepted academic practice. No use, distribution or reproduction is permitted which does not comply with these terms.